Tellus (1992), *44A*, 366–380

Numerical study of convective scale selection in a cloud-topped marine boundary layer

By BRIAN H. FIEDLER and STEVEN PECKHAM, *School of Meteorology, University of Oklahoma, 100 East Boyd # 1310, University of Oklahoma, Norman, OK 73019, USA*

(Manuscript received 6 November 1991; in final form 23 March 1992)

ABSTRACT

The conditions for the generation of broad convection cells in a cloud-topped, convective, marine atmospheric boundary layer are studied with an idealized two-dimensional model of non-precipitating moist convection. The inversion layer is represented by an elastic upper boundary rather than by the rigid lid that is often employed in these sorts of studies. A necessary condition for the formation of broad cells in the model is that either the convection penetrates the inversion by a distance at least half the average depth of the convecting atmospheric boundary layer, or that the rate of entrainment of dry inversion air is substantially reduced above cloud tops. The penetrative solutions display some similarity with mesoscale cellular convection observed during KONTUR, while the non-penetrative solutions display some similarity with AMTEX observations.

1. Introduction

Mesoscale cellular convection (MCC) is a ubiquitous phenomenon, yet a theoretical explanation for all instances of its development is still lacking. Nevertheless, there have been some advances in recent years. The fact that conditionally unstable convection tends to select broad scales is now fairly well established (Huang, 1990; Bretherton, 1988; Brugge and Moncrieff, 1985). However, a theory for the development of non-penetrative MCC in a convective atmospheric boundary layer (CABL) has not been widely accepted. The motivation for continuing to look for one is the same as in Fiedler (1984) and (1989), and will not be repeated here.

A two-dimensional numerical model is used to investigate the development of broad convective cells in a CABL. The model is very similar to that of Bretherton (1988) in that it uses constant eddy diffusivities and models non-precipitating convection that conserves mixing ratio and liquid water potential temperature. A novel feature of the model is that pressure forces within the convecting layer deflect the upper boundary. The model is idealized in the sense that the simplified constructions of physical processes allow for efficient design and computation of experiments that isolate cause and effect relationships. An alternative approach might be to use a three-dimensional model with a higher-order turbulence closure scheme like Hsu and Sun (1991). Such models are expensive to use, and, if broad cells do emerge in the model, the cause of their emergence is not necessarily easy to discern. Furthermore, such three-dimensional models are also approximate (that of Hsu and Sun is hydrostatic) and validation is still a major issue. Both idealized, two-dimensional models and state-of-the-art, three-dimensional models have a role to play in the science of atmospheric convection, just as they do in many other aspects of dynamical meteorology.

The first cell-broadening mechanism elucidated here requires that the overlaying inversion be weak enough to allow convection to penetrate into the inversion by a distance on the order of 0.5 H where H is the depth of the convective atmospheric boundary layer (CABL). (Excursions of cloud-top a distance of 0.3 H or more into the inversion will be referred to as "penetrative" in this paper. "Broad cells" will here mean a spacing between convective updrafts of at least 10 H). Compensating subsidence prevents weaker convective circulations from developing clouds and limits the number of convection cells. This mechanism is similar to that studied by Bretherton (1988, 1987),

except that in his model the cells become widely spaced only if the layer is *conditionally* unstable. Here the convective motion occurs in a layer that is *absolutely* unstable and thus the model is more applicable to boundary layer convection and MCC. Simulations are shown in which the cell-size gradually broadens from a 4:1 aspect ratio to a 30:1 aspect ratio typical of MCC. The mechanism could have been effective in the open cellular convection observed during KONTUR where the penetration was commonly in excess of 0.5 H (Brümmer et al., 1986). However, the current investigation indicates that this mechanism would not be effective in nonpenetrative convection under strong inversions as in AMTEX (Agee and Lomax, 1978).

The second and third mechanisms work with less penetration into the inversion but require the entrainment fluxes to exert a positive feedback on the mesoscale buoyancy fluctuations. These mechanisms are similar to the linear instability proposed by Fiedler (1984, 1985), but with nonlinear advection within the CABL now contributing. External positive feedback on buoyancy fluctuations is now known to be an especially effective agent for cell broadening in nonlinear convection (Fiedler, 1990). However, even allowing for speculative parameterizations that promote positive feedback, the model still falls somewhat short in predicting robust development of nonpenetrative MCC.

As in the earlier linear instability, the second mechanism requires the parameterization of a gravity current in the inversion that drains the most dense inversion air towards the troughs between clouds. The consequent *decrease* in the rate of entrainment above the cloudy regions reinforces the convection-scale humidity fluctuations and promotes additional latent heat release. These events constitute a positive feedback process that promotes cell broadening. With this second mechanism, the low-level humidity can be greater and the potential temperature less in the cloudy regions than in the clear regions, in accord with observations of nonpenetrative MCC in AMTEX (Rothermel and Agee, 1980, hereafter RA) and penetrative MCC in KONTUR (Brümmer et al., 1986).

The third mechanism requires that the penetrating clouds vigorously *increase* the rate of entrainment. Clouds thicken despite the fact that cloud-base rises because cloud-top rises faster. The thickened clouds promote an additional buoyancy flux from the inversion into the CABL, which in turn reinforces the mesoscale buoyancy fluctuations. The positive feedback loop is thus completed and broad cells emerge as in Fiedler (1990). However, the moisture and temperature fields are completely opposite the observations mentioned above.

2. The model

The model is a primitive-equation formulation of two-dimensional, incompressible thermal convection with constant eddy diffusivities, bounded from above and below by impermeable boundaries. The model explicitly represents only the largest convective scale fluctuations in a turbulent atmospheric boundary layer. The model plane is assumed to be orthogonal to any synoptic-scale wind in the boundary layer. The Boussinesq approximation is applied.

Except for the boundary conditions, the dimensionless model equations are exactly those of Bretherton (1988) but with a slightly more economical notation. The buoyancy is coupled to two conservative scalars, the liquid water potential temperature B and the mixing ratio C (the latter being first scaled by the latent heat of evaporation divided by specific heat). In constructing the model equations for B and C we first write $B = B_0(z, t) + b(x, z, t)$ and $C = C_0(z, t) + c(x, z, t)$ where B_0 and C_0 represents the diffusive solutions of B and C in the motionless state. The gradients of B_0 and C_0 are represented approximately by the constant parameters R and Q. The model equations in dimensionless form are:

$$\frac{\mathrm{d}b}{\mathrm{d}t} = Rw + \nabla^2 b, \tag{1}$$

$$\frac{\mathrm{d}c}{\mathrm{d}t} = Qw + \nabla^2 c, \tag{2}$$

$$\frac{\mathrm{d}u}{\mathrm{d}t} = -\frac{\partial p}{\partial x} + \nabla^2 u, \tag{3}$$

$$\frac{\mathrm{d}w}{\mathrm{d}t} = -\frac{\partial p}{\partial z} + \theta + \nabla^2 w, \tag{4}$$

$$\frac{\partial u}{\partial x} + \frac{\partial w}{\partial z} = 0. \tag{5}$$

The buoyancy fluctuation θ is due to b and due to condensation of liquid water mixing ratio s:

$$\theta = b + s. \tag{6}$$

Here s results from the excess of C above the saturation value, the latter which we take to vary linearly with z with proportionality constant $-\sigma$:

$$s = \max[c - (z_s - z)\,\sigma, 0]. \tag{7}$$

The value of z_s determines the height of the cloud base in the diffusive equilibrium state. It should be noted that though we use steady values for all parameters, the tendencies of C_0 and B_0 need not be zero; we are modeling the fluctuations in a mixed layer in which the mean state is evolving with time.

We take the lower boundary to be just above the surface layer. Application of bulk transfer models to the fluxes at the lower boundary leads to the following dimensionless relations for the flux fluctuations at the lower boundary:

$$\frac{\partial c}{\partial z} = \gamma c, \tag{8}$$

and

$$\frac{\partial b}{\partial z} = \gamma b, \tag{9}$$

where γ is a constant. The free-slip condition is applied at the upper and lower boundaries. The top of the CABL is at $\pi + \eta(x, t)$ where $\pi = 3.14...$ and η is modeled by the equation for a damped, nonlinear spring driven by pressure fluctuations at the top of the CABL:

$$K\frac{\mathrm{d}^2\eta}{\mathrm{d}t^2} + J\frac{\mathrm{d}\eta}{\mathrm{d}t} + G(1 + \mu\eta^2)\,\eta = p - \bar{p}. \tag{10}$$

The first term represents the inertia of the inversion, the second the damping of inversion height oscillations, the third the restoring force and the right-hand side is the forcing term. Here $\bar{p}$ is the horizontal average of p at the top boundary. One effect of the nonlinear term in the restoring force is that it prevents runaway penetration into the inversion. When we discuss the values for the constant parameters K, J, G and μ in Section 3 and the model integrations in Section 4, we will not claim that (10) is the correct or even best representation of the upper boundary, but simply that is much better than the ever-popular rigid lid.

The turbulent entrainment flux of B is $w_e\,\Delta B$ and of C is $w_e\,\Delta C$, where w_e is the dimensionless entrainment velocity. Here we use Δ as the conventional notation for the jump in a quantity across the inversion interface. For any CABL, we consider, $\Delta B > 0$, $\Delta C < 0$ and $w_e > 0$.

Clouds can cool a boundary layer by promoting upwards infrared radiation. Clouds can warm a boundary layer by absorbing solar radiation as well as by enhancing the entrainment of inversion air (e.g., Driedonks and Duynkerke, 1989). As the static stability of the entrainment interface increases, w_e decreases (Fiedler, 1984). As a consequence, in some clear CABL parameterizations, the entrainment flux of B is completely insensitive to ΔB. Here we assume this insensitivity extends to the cloud-topped regime; the horizontal fluctuations in the turbulent flux of B at the top of the CABL are modeled as being proportional only to fluctuations in the liquid water column density λ:

$$\frac{\partial b}{\partial z} = -\alpha\lambda, \tag{11}$$

where

$$\lambda = \int s\,\mathrm{d}z - 0.5\sigma(\pi - z_s)^2, \tag{12}$$

and α is a constant to be determined. The second term on the right in (12) is the column density of liquid water in the diffusive equilibrium state. Turbulence generated by latent heat release tends to make α negative. However, radiation effects can also be accounted for in (11). Incorporation of radiative effects into (11) would imply that all radiative flux divergences occur right at cloud-top. Although this approximation is certainly suspect, especially for solar radiation, its use should not alter the buoyancy budget within the CABL because of the large eddy diffusivity in the CABL. So here we also consider that absorption of solar radiation could tend to make α negative and infrared emission could tend to make α positive.

As the penetrating clouds come into contact

with warmer air in the stratified inversion layer, ΔB will increase and w_e will tend to decrease but ΔC will not change significantly. Thus the downwards flux of dry air will tend to decrease and the flux boundary condition for c should have a dependence on η that (11) did not have:

$$\frac{\partial c}{\partial z} = -\beta\lambda + \kappa\eta. \tag{13}$$

The values for β and κ will be assumed to be constant and non-negative. We do not claim that (11) and (13) would be the obvious first-choice for all people developing idealized models. However, we will show later that (11) and (13) efficiently allow for a much better approximation of reality than either a constant flux or a constant value boundary condition.

The numerical scheme uses second-order finite-differences on a mesh that stretches with the moving upper boundary. Second order finite-differences are applied to a mesh with uniform spacing in x and ξ, where:

$$z = \frac{\pi + \eta}{\pi}\,\xi. \tag{14}$$

Although $\chi \equiv x$ and $\tau \equiv t$, we have for any variable $f(\chi, \xi, \tau)$

$$\frac{\partial f}{\partial t} = \frac{\partial f}{\partial \tau} + \frac{\partial f}{\partial \xi}\frac{\partial \xi}{\partial t}, \tag{15}$$

$$\frac{\partial f}{\partial x} = \frac{\partial f}{\partial \chi} + \frac{\partial f}{\partial \xi}\frac{\partial \xi}{\partial x}, \tag{16}$$

$$\frac{\partial f}{\partial z} = \frac{\partial f}{\partial \xi}\frac{\partial \xi}{\partial z}, \tag{17}$$

where

$$\frac{\partial f}{\partial \tau} \equiv \left(\frac{\partial f}{\partial t}\right)_{x,\xi}, \tag{18}$$

$$\frac{\partial f}{\partial \chi} \equiv \left(\frac{\partial f}{\partial x}\right)_{t,\xi}. \tag{19}$$

Transformation of the model equations to the independent variables χ, ξ and τ is straight forward, and the implementation of a workable numerical scheme not difficult. The continuity equation was enforced approximately by using an iterative scheme to determine pressure.

3. Model parameters

MCC forms primarily over the oceans (Agee, 1987), suggesting that a small ratio of sensible heat flux to latent heat flux (the Bowen ratio) and small roughness length could be important factors in its formation. Agee and Dowell (1973) found the Bowen ratio did not exceed 0.12 in study of North Atlantic and North Pacific MCC. However, Sheu and Agee (1977) found that the Bowen ratio could be as high as 0.5 in MCC occurrences during AMTEX. The ratio R/Q should be roughly the Bowen ratio, or maybe less than the Bowen ratio because a negative buoyancy flux can occur near the top of the CABL. Here we will primarily use $R/Q = 0.25$.

The surface layer tends to insulate the bulk of the CABL from the ocean surface (Fiedler, 1989). Bulk transfer representation of the surface layer fluxes gives (Fiedler, 1984):

$$\gamma = \frac{HC_T U_{10}}{\pi K_{eddy}}. \tag{20}$$

As in Fiedler (1985), we will derive a value typical for AMTEX conditions. Large eddy models (Holtstag and Moeng, 1991) indicate that the most appropriate vertical eddy diffusivity value might be

$$K_{eddy} = \varepsilon w^* H, \tag{21}$$

where $0.1 < \varepsilon < 0.2$ and w^* is the convective velocity scale. The value of w^* in turn is about 0.6 times the root mean square velocity at mid-layer, which in RA can be seen to be of order 1 m s^{-1}. Here we will nondimensionalize the model with an isotropic eddy diffusivity $K_{eddy} = 300$ m^2 s^{-1}. Taking $H = 2$ km, the transfer coefficient $C_T = 1.5 \times 10^{-3}$, and the windspeed at 10 m height, $U_{10} = 10$ m s^{-1} yields $\gamma = 0.03$.

The Rayleigh number R in (1) is

$$R = -\frac{gH^4}{\Theta_0 \pi^4 K_{eddy}^2}\frac{dB_0}{dz}, \tag{22}$$

where Θ_0 is the mean value of potential temperature in the CABL. If we use eddy diffusivity to model the upwards heat flux then, in unsaturated conditions,

$$w^{*3} = -\frac{gHK_{\text{eddy}}}{\Theta_0}\frac{dB_0}{dz}, \tag{23}$$

$$R = \frac{1}{\varepsilon^3\pi^4}. \tag{24}$$

Here we will primarily use $R = 5$, which implies $\varepsilon = 0.127$. With $Q = 0$, the layer would be unstable with $R > 1.5$ (Fiedler, 1989). The cloud cover is relatively thin so even with $Q = 20$ the resolved convection is only slightly supercritical. The resolved velocities often come out to be of order 3 in the shorter-wavelength modes. The model has been nondimensionalized with velocity scale $\pi K_{\text{eddy}}/H$. This makes the dimensionless rms velocity implicit in the eddy diffusivity to be also of order 3. The cumulus-like convective modes are therefore consistent with being resolved "large-eddies" of comparable significance to the eddy transport modeled with the diffusion term. Thus, in an eddy-diffusivity model of a CABL, imposing slightly supercritical conditions appears to be the most consistent with the turbulent nature of the CABL.

The ratio σ/Q is the ratio of the saturation mixing ratio lapse rate to the mixing ratio lapse rate. Using 0.001 m^{-1} for the latter as in Fiedler (1984) and 0.01 m^{-1} for the former gives $\sigma/Q = 10$; here we will use $\sigma = 200$ and $z_s = 0.8\pi$. The ratio G/R should be on the order of the ratio of the temperature jump across the inversion interface to the liquid water potential temperature change across the CABL; it will also be the ratio of the temperature jump across the inversion interface to the mesoscale fluctuation in liquid water potential temperature in the CABL. This ratio should be at least 10 and in the standard experiment we use $G = 180$, which is approximately $10\pi R$. Furthermore we take $\mu = 0.5$ to represent a doubling in the interfacial buoyancy jump as a cloud penetrates a dimensionless distance of 1.4 into the stably stratified inversion.

The value of K roughly represents the depth of the inversion participating in the deflections; here we take $K = 5$. A value of $J = 25$ makes the damping time comparable to the period of oscillation for the values of G that will be used. The damping process presumably could be due to gravity wave radiation.

Appropriate values of α, β and κ are as difficult to estimate. Fiedler (1984) presented a tortuous derivation of a parameterization for mesoscale fluctuations in the entrainment rate in an attempt to demonstrate that the entrainment fluxes could reinforce both the mesoscale mixing ratio *and* the liquid water potential temperature fluctuations. Indeed, the significant conclusion of Fiedler (1984) was that, if conventional entrainment notions were accepted, such reinforcement, or positive feedback, would be rare and weak. A similar inquiry into entrainment rates is probably not worthwhile here because, first of all, many of the premises of such a derivation are still questionable. Furthermore, even when we give the positive feedback mechanisms the benefit of the doubt, the model still does not adequately predict the evolution of nonpenetrative MCC, although it is considerably improved over that of Fiedler (1984).

In many of the penetrative experiments the values for α and β are chosen to keep the *damping* time scales for b and c from the upper boundary conditions comparable to the time scales derived from the lower boundary conditions. All such time scales are significantly greater than the diffusion time, which in this dimensionless model is unity; both the upper and lower boundary conditions are close to being constant flux boundary conditions. In the standard experiment, $\alpha = 0.05$, $\beta = 0.2$ and $\kappa = 0$. These parameters imply that enhanced infrared cooling by clouds is greater than the enhanced heating by solar absorption and entrainment and that the clouds promote more entrainment of dry inversion air, both processes are negative feedback processes. The effect of a range of values for α and β will be explored and in some instances we consider $\alpha < 0$, or that clouds warm the CABL. We also consider some cases where $\kappa > 0$ so penetration can decrease the entrainment rate and as a consequence the fluctuations in the entrainment flux reinforce the mixing ratio fluctuations. A rigorous justification for a value for κ would have to be based on properties of gravity currents in the inversion and on turbulence (Fiedler, 1984). No attempt will be made here to offer a satisfactory degree of rigor because it would greatly lengthen the presentation. As we shall see,

Table 1. *Dimensionless model parameters, standard values and the equation where they first appear*

Parameter	Standard value	Eq.
R: "Rayleigh number" for sensible heat	5	1
Q: "Rayleigh number" for latent heat	20	2
σ: saturation mixing ratio lapse rate	200	7
z_s: equilibrium cloud base	0.8π	7
γ: lower boundary flux parameter	0.03	8
K: inertial depth of inversion	5	10
J: damping coefficient of inversion	25	10
G: inversion interfacial stability	180	10
μ: nonlinear restoring force coefficient	0.5	10
α: upper boundary heat flux parameter	0.05	11
β: upper boundary mixing ratio flux parameter	0.2	13
κ: upper boundary mixing ratio flux parameter	0.0	13

the model integrations themselves put limits on the magnitudes of κ that can be considered and much can be learned by simply invoking values for κ.

4. Model integrations

All experiments are initialized with the same initial random perturbation. The ratio of width to height is $20\sqrt{2}$, as in Rothermel and Agee (1986). The boundary conditions are periodic. The numerical grid has 25 points in the vertical and 129 in the horizontal. One convection cell in the domain would correspond to typical MCC aspect ratio or spacing. The model equations are integrated from $t=0$ to $t=100$ or, in some cases, to $t=200$. One unit of dimensionless time corresponds to 1350 s in AMTEX conditions, so $t=100$ would correspond to 1.56 days.

The standard experiment will be designated G180. The values of the standard parameters are listed in Table 1. Descriptions of some selected variables are reiterated in Table 2. The label for all experiments will indicate any values for parameters that have been substituted for the standard values. For example, G240 uses $G=240$ instead of $G=180$; $\kappa 60 G350 z_s 0.7\pi$ uses $\kappa=60$, $G=350$ and $z_s=0.7\pi$.

Fig. 1 is a plot of $\lambda(x, t)$ for the experiments where the broadening appears to be linked to the first mechanism, i.e., penetration. As the inversion interface becomes less stable, that is as G is decreased from 240 to 180, the stable distribution of eight cells gives way to a pulsating array of cells in which only two cells or two clusters are predominant at a given time, to a single cluster in G180. (A cluster is defined as the persistence of two or more convective entities within a distance less than one-half the largest gap between convective entities. Clustering is defined as tendency for convective entities to move into clusters). Clustering does not persist in G160 where the cell evolution has become erratic. At some times in G160, the cell pattern could be interpreted as containing a single cluster (e.g., $t=80$). At other times, there are up to three uniformly distributed cells (e.g., $t=100$). The contour plots of $s(x, z)$ at $t=100$ in Fig. 2 show the increasing penetration and broadening as G is decreased. The issue of what values of G and μ are appropriate can now be adequately addressed simply by inspecting the degree of penetration they allow for.

Table 2. *Selected dimensionless model variables and the equation where they first appear*

Variable	Eq.
B: liquid water potential temperature	—
b: liquid water potential temperature fluctuation	1
C: water mixing ratio	—
c: water mixing ratio fluctuation	1
θ: buoyancy	4
s: liquid water mixing ratio	6
λ: liquid water column density	12

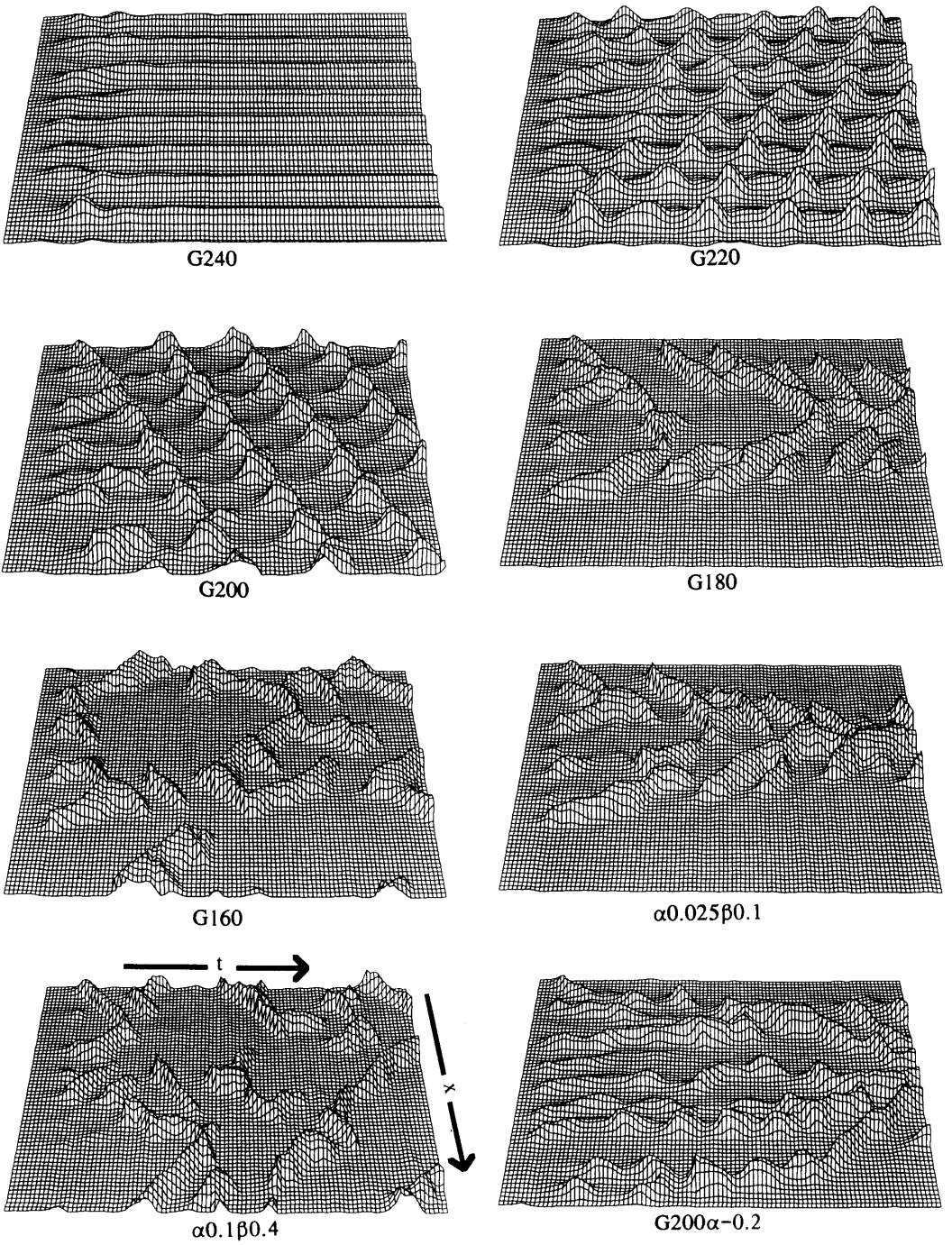

Fig. 1. Fluctuation in liquid water column density $\lambda(x, t)$ for the experiments where penetration and compensating subsidence appear to be responsible for any cell broadening. The vertical scale is arbitrary.

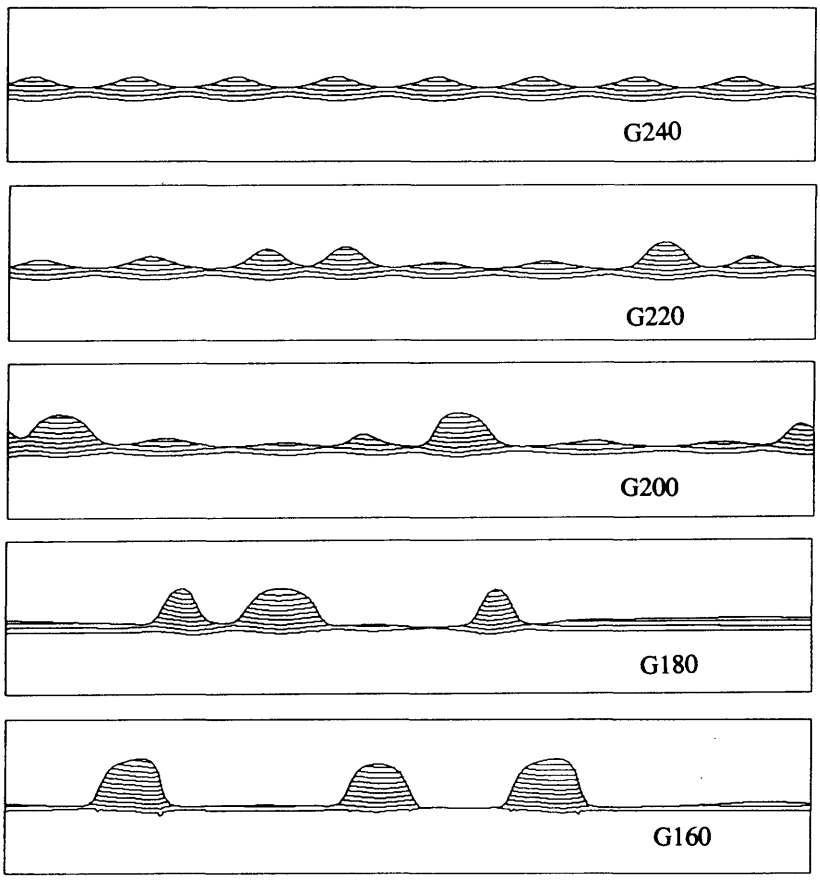

Fig. 2. Liquid water $s(x, z)$ at $t = 100$ in selected experiments with decreasing inversion interface stability.

Contour plots of w, b, c and s at $t = 100$ for G180 are shown in Fig. 3. Note that $c/b = Q/R$ as a consequence of using $\beta/\alpha = Q/R$. (In other cases, with different upper boundary conditions, the fields for c and b can be quite dissimilar.) Although the solution is reminiscent of several cumulus entities clustering together to form one MCC cell, there are several features of this solution that are not in accord with AMTEX observations. First, the driest and coldest low-level air in the solution is beneath the cloud cluster. Although the aircraft data of RA shows that the coldest air may be beneath the cloudy region, a large humidity fluctuation, of magnitude as large as the change in mixing ratio between the bottom and top of the CABL, exists in phase with the cloudy regions throughout the depth of the CABL. Second, in the solution the convection penetrates into the inversion a distance of 0.5 H. Agee and Lomax (1978) show that the penetration of the AMTEX MCC was only about 0.1 H. Although penetrative MCC does exist in nature, the extensive penetration necessary for MCC to occur in the first set of experiments is not a necessary condition in nature. Lastly, the resolved velocity field is almost completely shut down outside the cluster. This, however, does not mean that the model is predicting no convective motion outside the cluster, but rather that the model does not predict convective motion in excess of that implied by the eddy diffusivity. The lack of a resolved velocity field leaves a thin layer of undisturbed stratus cloud rather than patchy or broken clouds. Nevertheless, we still interpret G200, G180 and G160 as

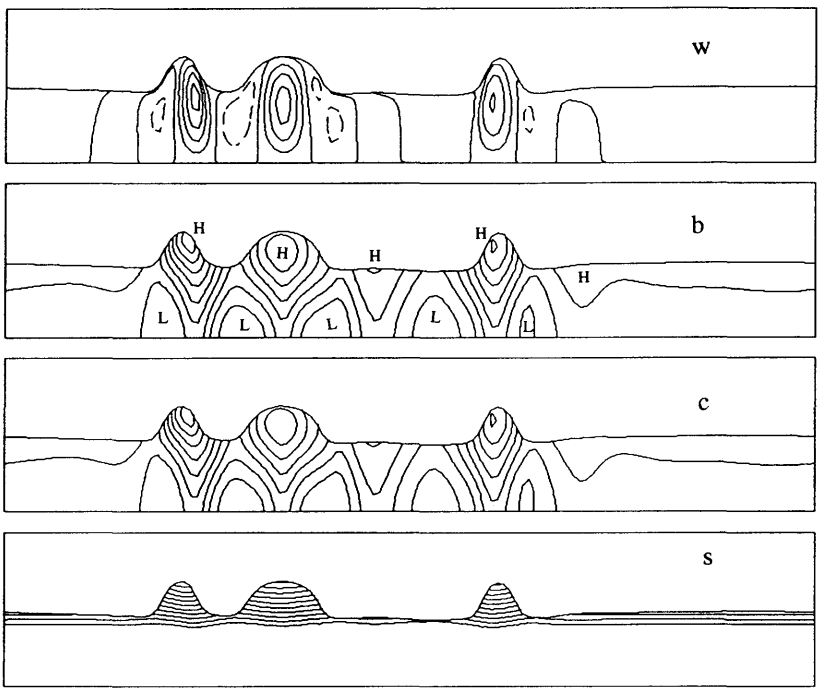

Fig. 3. $w(x, z)$, $b(x, z)$, $c(x, z)$ and $s(x, z)$ at $t = 100$ in G180. Contour intervals are 1, 2.5, 10 and 40 respectively. Solid contours are positive, dashed contours are negative.

representing "open" cells. The use of a slightly higher value of z_s, as well as representation of patchiness of the thin clouds, would probably render images more in accord with readers' expectations of what open cells should look like: a thick cloud deck covering less than 50% of the area.

We now turn to exploring the sensitivity of the model to values for α and β. Experiment $\alpha 0.025 \beta 0.1$ displays clustering like that in G180, except the final cluster is narrower and more steady (Fig. 1). In Experiment $\alpha 0.1 \beta 0.4$ the clustering is more erratic and similar in behavior to G160. It appears that the less the boundary fluxes detract from the convective fluctuations, the greater the tendency to form broad scales. This tendency is in accord with the properties of simpler Rayleigh-Bénard models of convection (Fiedler, 1989). In $G200\alpha - 0.2$ the negative value for α implies that the downwards flux of buoyancy induced by the cloud is greater than the cloud-top cooling. The pulsations that occurred in G200 have decreased and the evolution is similar to G180. But perhaps the reason for this is that the positive feedback on the buoyancy fluctuations caused more penetration and made the dynamics similar to G180.

Next we mention two control experiments with no clouds: $\lambda = 0$ and $s = 0$. In the first we take $R = 10$ and $G = 30$ and otherwise as in G180. The convection settles down into a uniform array of 10 cells by $t = 20$ with the peak values of η slightly larger than the largest in G220. In the second we use also a rigid lid. The convection settles into a uniform array of 8 cells by $t = 20$. The control experiments indicate the necessity of latent heat release near the top of the boundary if the convection is to broaden; an elastic top boundary by itself is not a sufficient condition.

We also applied a rigid lid and constant value or constant flux boundary conditions as in Bretherton (1988) to verify the model in that limit. For instance, using $Q = 60$, $R = -30$ and $\sigma = 0$ with boundary conditions $b = c = 0$ corresponds to Bretherton's [Fig. 8]. We confirmed his result that conditionally unstable layers tend to select widely

spaced convection; we also showed that as R becomes less negative and then positive this property disappears, as in G240.

As mentioned above, the cluster in G180 is excessively drying the CABL. This indicates that a lesser value for β might be more realistic. Here we will invoke a positive value for κ and achieve the same effect. Fig. 4 is a plot of $\lambda(x, t)$ for the remaining experiments where the entrainment fluxes have a crucial effect on the broadening. Contour plots of w, b, c and s at $t = 100$ for $\kappa 60 G350 z_s 0.7\pi$ are shown in Fig. 5. The contours of c clearly indicate that the fluctuating flux at the top boundary is reinforcing the mesoscale humidity fluctuation associated with the cloudy region. In contrast with G180, the subcloud temperature field and humidity field are now in accord with RA. The temperature field even displays the distinctive "double-cycle" variation at low-levels identified by RA. The ratio of the mesoscale c fluctuations to the mesoscale b fluctuations is about -5; which is also similar to that shown in RA. Likewise the mesoscale c fluctuation is greater than the difference in C across the depth of the CABL, which is also in accord with the observations, if we compare RA with the sounding in Jensen and Lenschow (1978). Indeed, it is this large mesoscale humidity fluctuation that is so difficult to reproduce without a decrease in the rate of entrainment above penetrating clouds and it is the feature upon which we should focus serious attention. Perhaps rain could also have contributed to the sub-cloud temperature field in RA as it did in FIRE (Paluch and Lenschow, 1991), and rain is not included in this model.

Nevertheless, there are some unrealistic features of $\kappa 60 G350 z_s 0.7\pi$. The penetration is still rather large for an AMTEX case. Moreover, with $\partial C_0/\partial z = -Q$ and $\partial c/\partial z$ as large as 34 near cloud-top gives $\partial C/\partial z$ as large as 14 near cloud-top in some places, which implies that we have more than shut down the drying entrainment flux, we have actually reversed it in some places! Such are the pitfalls of idealized models. Simply reducing κ was not an adequate way to repair this feature and yet preserve realistically rapid cell broadening.

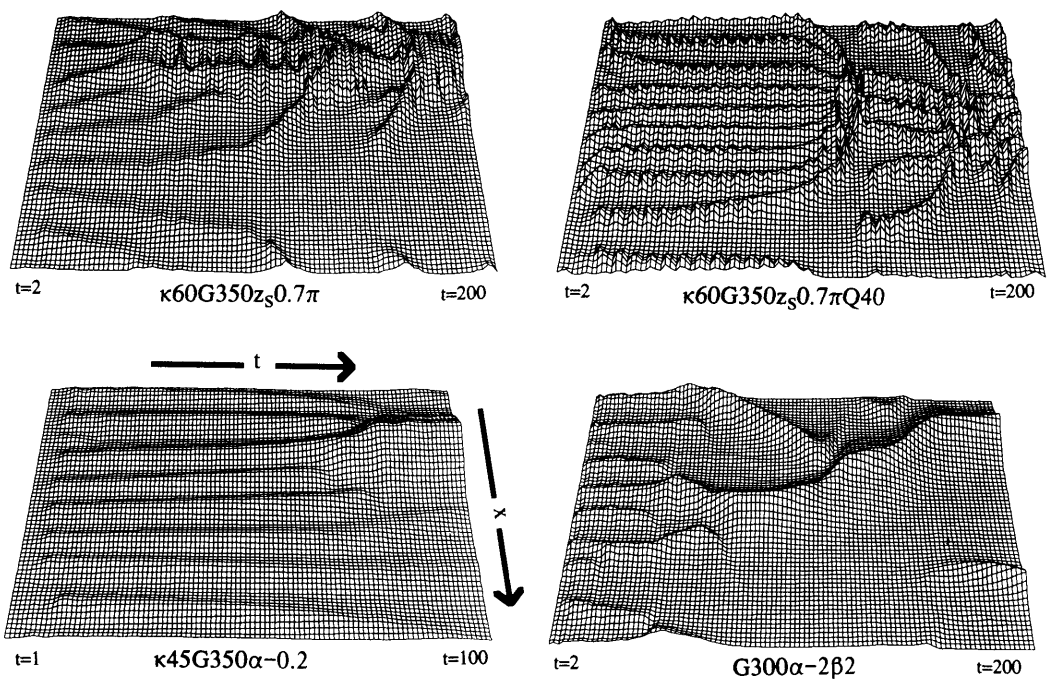

Fig. 4. As in Fig. 1, but for experiments where positive feedback by entrainment appears to be responsible for any cell broadening.

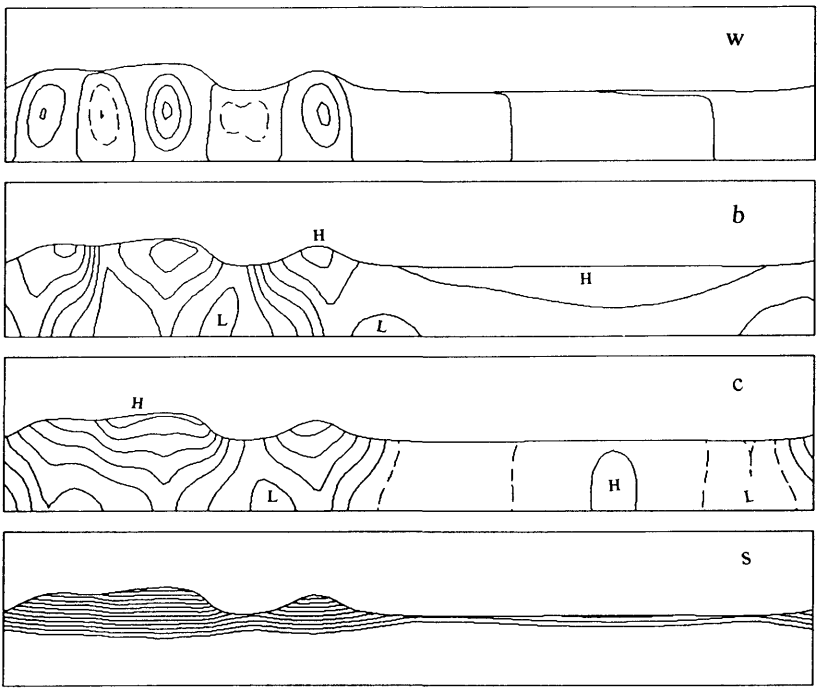

Fig. 5. $\kappa 60G350z_s 0.7\pi$ at $t = 200$. Contour intervals for w, b, c and s are 1, 5, 20 and 40.

Perhaps this is because the model does not include the virtual effects of water vapor on buoyancy and therefore the model requires excessive cloud buoyancy to overcome the subcloud negative buoyancy. So in $\kappa 45G350\alpha - 0.2$ (Fig. 6) the source of the sub-cloud negative buoyancy is removed by taking a negative value for α. At $t = 100$, we have $\partial C/\partial z < -1.5$ at the top of the CABL, so the entrainment velocity is nearly zero at some cloud peaks, but at least still positive. The negative value for α implies that the cloud is promoting an enhanced downwards buoyancy flux, which could be ascribed to enhanced absorption of solar radiation, or, as in Fiedler (1984), enhanced entrainment of B. The case $\kappa 45G350\alpha - 0.2$ is in fact the only one presented here in which both upper boundary fluxes are acting as in the instability described in Fiedler (1984).

An alternative repair is in $\kappa 60G350z_s 0.7\pi Q40$ (Fig. 7). Here $\partial C/\partial z < -7$ at the top of the CABL, which implies that the entrainment velocity has been reduced to as little as 18% of the mean value at the top of the thickest cloud. Again at low-levels, the subcloud region contains the coldest and most humid air. Furthermore, the relatively broad cap of thick cloud cover for $t < 100$ was similar to that of closed cellular convection, while the narrower cap of thick cloud cover for $t > 100$ is similar to that of open cellular convection.

The model integrations now can now be used to address the issue about the appropriate value for κ. A good question to ask now is whether or not w_e can be reduced to near zero above a cloud-top that has penetrated or deflected the inversion by a mere 300 m, say. The answer is probably not. With their great reduction in entrainment above penetrating clouds, all three experiments with $\kappa > 0$ scenario imply extremely (and probably unnaturally) stable stratification within the inversion layer, a result consistent with Fiedler (1984). Nevertheless some of the features of the solutions are intriguing.

Lastly, we again consider, as in $G200\alpha - 0.2$, that the clouds induce a downwards flux of dry and buoyant air. In $G300\alpha - 2\beta 2$ (Fig. 8) these downwards fluxes will be enhanced by a factor

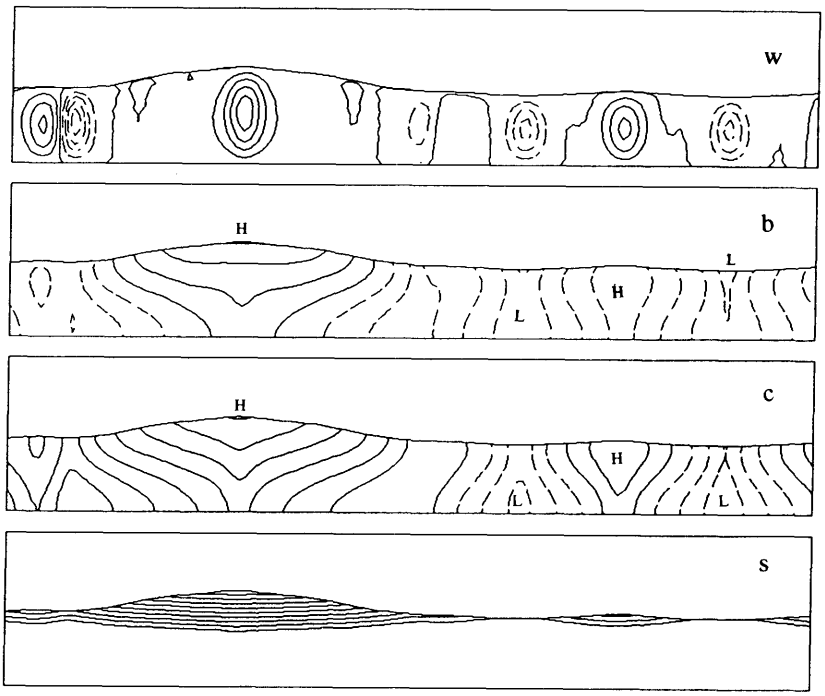

Fig. 6. $\kappa 45G350\alpha - 0.2$ at $t = 100$. Contour intervals for w, b, c and s are 0.5, 10, 20 and 40.

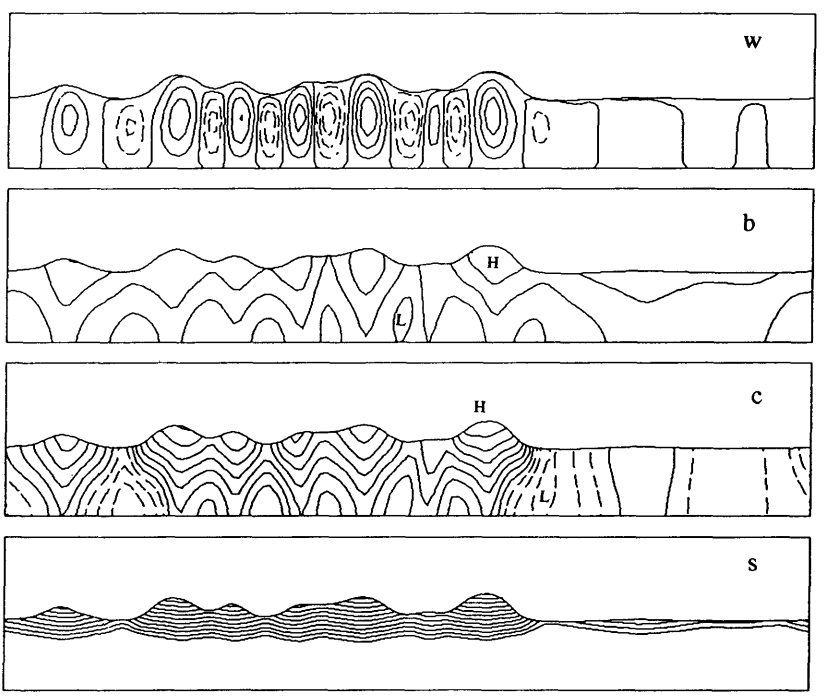

Fig. 7. $\kappa 60G350z_s 0.7\pi Q40$ at $t = 200$. Contour intervals for w, b, c and s are 1, 5, 20 and 40.

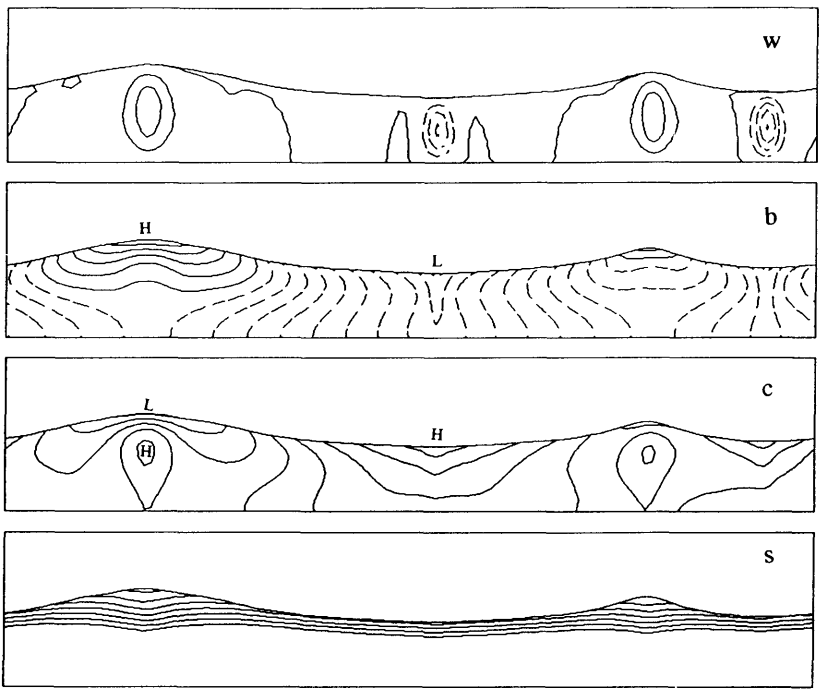

Fig. 8. $G300\alpha - 2\beta 2$ at $t = 200$. Contour intervals for w, b, c and s are 1, 20, 20 and 40.

of 10, and the penetration effect will be lessened. Conditions would probably have to be ripe for cloud-top entrainment instability if the entrainment rate were to be this sensitive to the presence of liquid water at the CABL top. The conditions for buoyancy reversal and cloud-top entrainment instability as laid down by Randall (1980) and Deardorff (1980) are nearly:

$$\frac{\Delta C_0}{\Delta B_0} < -1, \tag{25}$$

while the modeling of Siems et al. (1989) implies that a runaway instability could occur only if

$$\frac{\Delta C_0}{\Delta B_0} < -2.4, \tag{26}$$

and even then only if sufficient liquid water was present in the cloud. The fluctuating fluxes of c and b due to a fluctuation in the entrainment velocity should be roughly proportional to $\Delta C_0/\Delta B_0$. In $G300\alpha - 2\beta 2$ we take $\alpha/\beta = -1$, which though inconsistent with (26), seemed to prevent excessive drying of the cloudy regions. The drying effect of enhanced entrainment trends to raise cloud base, however penetrating clouds still deepen because the height of the cloud top is increased, a process described in Randall (1984). The deflection of the inversion and thicker cloud cover is now correlated with regions where the sub-cloud air is dry and buoyant, which is completed opposite with the situation reported in RA.

5. Conclusion

Here we have seen that absolutely unstable convection can select broad scales. However such selection occurred in the first set of experiments only as we adjusted G towards a regime where significant buoyancy production was occurring in excursions above the mean CABL top, or after we had in a sense "made the inversion conditionally unstable". As a consequence of the low Bowen ratio, the thin cloud layer is an important source of convective scale buoyancy fluctuations. At least in the linear theory, a given vertical velocity

generates 5 × as much buoyancy in the cloud-layer as beneath it for $Q/R = 4$. Thus the convection will be sensitive to cloud layer thickness, which is obviously very sensitive to deflections of the inversion. Sykes et al. (1988) also observed broad spacing in a numerical simulation of penetrating boundary layer convection. They identify entrainment of buoyancy by the cloud as crucial for producing large aspect ratios; however they did not conduct and experiment that would isolate the entrainment effect from the penetration effect.

The clustering that occurred in some of the penetrative simulations involved the regeneration of a penetrative entities in the relative dry and thin-cloud region near the cluster that then travel inwards towards the center of the cluster. This phenomenon defies a simple explanation. However, the fact that broadly spaced cells occurred is not unexpected in light of Huang (1990), Bretherton (1988) and Brugge and Moncrieff (1985).

Experiments with $\kappa > 0$ are able to reproduce some important featues of AMTEX MCC, but the requirement of an efficient "mountain breeze in the sky" that drains the most dense inversion air a distance of 10 km down a slope of several hundred meters is certainly unorthodox (if not incredible). This inversion flow could in principal be explicitly resolved in a numerical model like that of Sykes et al. (1988) if the numerical model requirements are addressed with care. (Indeed, maybe it did occur in their simulations). Nevertheless, there are good reasons to suspect that this inversion flow might not be effective. The necessity of very stable stratification has already been mentioned. Another is that any shear across the inversion interface might easily disrupt the effectiveness of this transport, unless the convection was organized as cloud streets aligned with the shear across the inversion interface. As far as we are concerned, a succinct and convincing explanation for the development of non-penetrative MCC has yet to be formulated.

6. Acknowledgement

This research was supported in part by NSF grant ATM-9002391.

REFERENCES

Agee, E. M. 1987. Mesoscale cellular convection over the oceans. *Dyn. Atmos. Oceans 10*, 317–341.

Agee, E. M. and Dowell, K. E. 1974. Observational studies of mesoscale cellular convection. *J. Appl. Met. 13*, 46–71.

Agee, E. M. and Lomax, F. E. 1978. Structure of the mixed layer and inversion layer associated with patterns of mesoscale cellular convection during AMTEX 1975. *J. Atmos. Sci. 35*, 2281–2301.

Bretherton, C. S. 1987. A mathematical model of non-precipitating convection between two parallel plates. Part I: "Linear" theory and cloud structure. *J. Atmos. Sci. 44*, 1809–1827.

Bretherton, C. S. 1988. A theory for nonprecipitating convection between two parallel plates. Part II: Nonlinear theory and cloud field organization. *J. Atmos. Sci. 45*, 2391–2415.

Brugge, R. and Moncrieff, M. W. 1985. The effect of physical processes on numerical simulations of two-dimensional cellular convection. *Beitr. Phys. Atmosph. 58*, 417–440.

Brümmer, B., Fischer, T. and Zank, S. 1986. Aircraft observations of open cellular structures during KonTur. *Beitr. Phys. Atmosph. 59*, 162–184.

Deardorff, J. W. 1980. Cloud-top entrainment instability. *J. Atmos. Sci. 37*, 131–146.

Driedonks, A. G. M. and Duynkerke, P. G. 1989. Current problems in the stratocumulus-topped atmospheric boundary layer. *Bound.-Layer Meteor. 46*, 275–304.

Fiedler, B. H. 1984. The mesoscale stability of entrainment into cloud-topped mixed layers. *J. Atmos. Sci. 41*, 92. (Corrigenda, p. 1475)

Fiedler, B. H. 1985. Mesoscale cellular convection: Is it convection? *Tellus 37A*, 163–175.

Fiedler, B. H. 1989. Scale selection in nonlinear thermal convection between poorly conducting boundaries. *Geophys. & Astrophys. Fluid Dyn. 46*, 191–201.

Fiedler, B. H. 1990. Transitions to broad cells in a nonlinear thermal convection system. *Geophys. & Astrophys. Fluid Dyn. 50*, 195–201.

Holtslag, A. A. M. and Moeng, C. H. 1991. Eddy diffusivity and countergradient transport in the convective atmospheric boundary layer. *J. Atmos. Sci. 48*, 1690–1698.

Hsu, W. R. and Sun, W. Y. 1991. Numerical study of mesoscale cellular convection. *Boundary-Layer Meteorol. 57*, 167–186.

Huang, X. Y. 1990. The organization of moist convection by internal gravity waves. *Tellus 42A*, 270–285.

Jensen, N. O. and Lenschow, D. H. 1978. An observational investigation of penetrative convection. *J. Atmos. Sci. 35*, 1924–1933.

Paluch, I. R. and Lenschow, D. H. 1991. Stratiform cloud

formation in the marine boundary layer. *J. Atmos. Sci. 48*, 2141–2158.

Randall, D. A. 1980. Conditional instability of the first kind upside-down. *J. Atmos. Sci. 37*, 125–130.

Randall, D. A. 1984. Stratocumulus cloud deepening through entrainment. *Tellus 36A*, 446–457.

Rothermel, J. and Agee, E. M. 1980. Aircraft investigation of mesoscale cellular convection during AMTEX 75. *J. Atmos. Sci. 37*, 1027–1409.

Rothermel, J. and Agee, E. M. 1986. A numerical study of atmospheric convective scaling. *J. Atmos. Sci. 43*, 1185–1197.

Siems, S. T., Bretherton, C. S., Baker, M. B., Shy, S. and Breidenthal, R. E. 1990. Buoyancy reversal and cloud-top entrainment instability. *Q. J. R. Meteorol. Soc. 116*, 705–739.

Sheu, P. J. and Agee, E. M. 1977. Kinematic analysis and air-sea heat flux associated with mesoscale cellular convection during AMTEX 75. *J. Atmos. Sci. 34*, 793–801.

Sykes, R. I., Lewellen, W. S. and Henn, D. S. 1988. A numerical study of the development of cloud-street spacing. *J. Atmos. Sci. 45*, 2556–2569.